

Controlling Continuous Relaxation for Combinatorial Optimization

Yuma Ichikawa^{1,2}

Abstract

Motivated by developments in machine learning technologies, unsupervised learning (UL)-based solvers for CO problems have recently been proposed. These solvers train a neural network that outputs a solution by optimizing the CO objective directly. UL-based solvers have several advantages over traditional methods. However, various studies have shown that these solvers underperform compared to greedy algorithms for complex CO problems. In addition, these solvers employ a continuous relaxation strategy; thus, post-learning rounding from the continuous space back to the original discrete space is required, undermining the robustness of the results. To address these problems, we propose the continuous relaxation annealing (**CRA**) strategy. The CRA introduces a penalty term to control the continuity and discreteness of the relaxed variables and eliminate local optima. In addition, the CRA implements an annealing process for the penalty term that initially prioritizes continuous solutions and progressively transitions towards discrete solutions until the relaxed variables become nearly discrete, eliminating the artificial rounding. Experimental results demonstrate that the CRA significantly enhances the UL-based solvers, outperforming both existing UL-based solvers and greedy algorithms for complex CO problems.

1. Introduction

The objective of combinatorial optimization (CO) problems is to find the optimal solution from a discrete space, and CO problems are fundamental in many real-world applications, e.g., transportation logistics, scheduling, network design, and energy management (Glover et al., 2019; Kochenberger et al., 2014; Anthony et al., 2017; Papadimitriou & Steiglitz, 1998; Korte et al., 2011). Most CO problems are NP-hard

¹Fujitsu Limited ²University of Tokyo. Correspondence to: Yuma Ichikawa <ichikawa.yuma@fujitsu.com, ichikawa-yuma1@g.ecc.u-tokyo.ac.jp>.

or NP-complete; thus, solving large-scale problems within feasible computational time can be challenging. Traditional methods frequently depend on heuristics to find approximation solutions. However, considerable insights into the particular problems are required.

Recently, several studies have used machine learning methods to handle CO problems by learning heuristics, and such techniques are referred to as learning for CO (LCO) approaches. Most studies focus on supervised learning (SL)-based solvers (Hudson et al., 2021; Joshi et al., 2019; Gasse et al., 2019; Selsam et al., 2018; Khalil et al., 2016), which require optimal solutions for the CO problems as training labels. However, SL-based solvers have faced criticism for requiring extensive amounts of optimal solutions as supervision. Moreover, the models frequently result in overfitting (Kool et al., 2018; Yehuda et al., 2020). On the other hand, reinforcement learning (RL)-based solvers (Mazyavkina et al., 2021; Kwon et al., 2020; Yao et al., 2019; Chen & Tian, 2019; Yolcu & Póczos, 2019; Nazari et al., 2018; Khalil et al., 2017; Bello et al., 2016) do not require such optimal solutions but frequently suffer from unstable learning processes (Mnih et al., 2015). Recently, unsupervised learning (UL)-based solvers have attracted increasing attention (Wang et al., 2022; Schuetz et al., 2022a; Karalias & Loukas, 2020; Amizadeh et al., 2018). UL-based solvers follow a continuous relaxation approach, training a UL model to output a “soft” solution to the relaxed CO problem by directly optimizing the differentiable objective function. UL-based solvers offer significant advantages, including stable and fast training and a remarkable ability to handle large-scale CO problems. Notably, physics-inspired GNN (PI-GNN) solver (Schuetz et al., 2022a;b), which is a UL-based solver employing graph neural networks (GNN), performs on par with or outperforms existing solvers for CO problems with millions of variables.

While UL-based solvers offer some advantages over traditional and machine learning-based solvers, they confront two practical issues that must be considered. The first issue is related to their performance. Recently, Angelini & Ricci-Tersenghi (2023) demonstrated that the PI-GNN solver (Schuetz et al., 2022a) could not achieve results comparable to those of the degree-based greedy algorithm (DGA) (Angelini & Ricci-Tersenghi, 2019) in maximum independent set (MIS) problems on random regular graphs (RRG).

They also pointed out the necessity for discussions regarding the effectiveness of UL-based solvers, especially in more complex CO problems where the performance of greedy algorithms worsens. Moreover, Wang & Li (2023) pointed out that the PI-GNN solver tends to be trapped in local optimum because it is directly optimized for each instance without using historical data. In deed, this study also numerically observes that, as the graph becomes denser, the PI-GNN solver struggles to find valid solutions due to a local optimum during the early learning stages. This issue is a crucial bottleneck for its applicability in various real-world applications. The second issue relates to the inherent ambiguity in the continuous relaxation approach. This approach requires artificial rounding from the soft solution, which may include continuous values, back to the original discrete solution, potentially undermining the robustness of the results. Indeed, while linear relaxation can provide an optimal solution for original discrete problems on bipartite graphs (Hoffman & Kruskal, 2010), it typically leads to solutions with $1/2$ values, which is known to half-integrality (Nemhauser & Trotter Jr, 1974). In such cases, existing rounding methods completely lose their robustness.

To address these issues, we propose the continuous relaxation annealing (CRA) strategy. The CRA introduces a penalty term to control the continuity and discreteness of the relaxed variables, with a parameter γ to regulate the intensity of this penalty term. If the parameter γ is small, the relaxed variable tends to favor continuous solutions. In contrast, a large γ value leads the relaxed variables to favor the discrete space. This penalty term also effectively eliminates local optimum. Moreover, a small γ forces the loss function to approach a simple convex function, encouraging active exploration in the continuous space. The CRA also includes an annealing process, where γ is increased progressively until the relaxed variables are nearly discrete values, eliminating the artificial rounding from the continuous to the original discrete space after learning. In this study, the solver that applies the CRA to the PI-GNN solver is referred to as the CRA-PI-GNN solver.

We also demonstrate the benefits of the CRA through experiments on benchmark CO problems, including MIS, maximum cut (MaxCut), and diverse bipartite matching (DBM) problems across graphs of varying sizes and degrees. The experimental results show that the CRA significantly enhances the performance of the PI-GNN solver, outperforming the original PI-GNN solver, other state-of-the-art learning-based baselines, and greedy algorithms. This improvement is achieved by directly optimizing each instance without any history, e.g., previous optimal solutions and the information of other instances. Additionally, these experiments indicate that the CRA accelerates the learning process of the PI-GNN solver. Notably, these results overcome the limitations pointed out by Angelini & Ricci-Tersenghi

(2023); Wang & Li (2023), highlighting the further potential of UL-based solvers.

Notation. We use the shorthand expression $[N] = \{1, 2, \dots, N\}$, $N \in \mathbb{N}$. Here, $I_N \in \mathbb{R}^{N \times N}$ denotes an $N \times N$ identity matrix, $\mathbf{1}_N$ denotes the vector $(1, \dots, 1)^\top \in \mathbb{R}^N$, and $\mathbf{0}_N$ denotes the vector $(0, \dots, 0)^\top \in \mathbb{R}^N$.

CO Problems. The goal of this study is to solve the following constrained CO problem.

$$\min_{\mathbf{x} \in \{0,1\}^N} f(\mathbf{x}; C) \quad \text{s.t.} \quad \mathbf{x} \in \mathcal{X}(C), \quad (1)$$

where $C \in \mathcal{C}$ denotes instance parameters, e.g., a graph $G = (V, E)$, where V is the node set, and E is the edge set, and $f : \mathcal{X} \times \mathcal{C} \rightarrow \mathbb{R}$ represents the cost function. In addition, $\mathbf{x} = (x_i)_{1 \leq i \leq N} \in \{0, 1\}^N$ is a binary vector to be optimized, and $\mathcal{X}(C) \subseteq \{0, 1\}^N$ is the space of feasible solutions, typically specified by the following equality and inequality constraints.

$$\begin{aligned} \mathcal{X}(C) = \{ \mathbf{x} \in \{0, 1\}^N \mid & \forall i \in [I], g_i(\mathbf{x}; C) \leq 0, \\ & \forall j \in [J], h_j(\mathbf{x}; C) = 0 \} \end{aligned}$$

Here, for $i \in [I]$, $g_i : \{0, 1\}^N \times \mathcal{C} \rightarrow \mathbb{R}$ is the inequality constraint, and for $j \in [J]$, $h_j : \{0, 1\}^N \times \mathcal{C} \rightarrow \mathbb{R}$ is the equality constraint.

Penalty Method. The penalty method (Smith et al., 1997) in CO problems is used to handle constraints by incorporating them into the objective function as a penalty term as follows.

$$\min_{\mathbf{x}} l(\mathbf{x}; C, \boldsymbol{\lambda}), \quad l(\mathbf{x}; C, \boldsymbol{\lambda}) \triangleq f(\mathbf{x}; C) + \sum_{i=1}^{I+J} \lambda_i v_i(\mathbf{x}; C). \quad (2)$$

Here, for all $i \in [I+J]$, $v : \{0, 1\}^N \times \mathcal{C} \rightarrow \mathbb{R}$ is the penalty term, which increases the value when the constraints are violated, e.g., the penalty term is defined as follows:

$$\begin{aligned} \forall i \in [I], v_i(\mathbf{x}; C) &= \max(0, g_i(\mathbf{x}; C)) \quad [\text{Inequality}], \\ \forall j \in [J], v_j(\mathbf{x}; C) &= (h_j(\mathbf{x}; C))^2 \quad [\text{Equality}], \end{aligned}$$

and $\boldsymbol{\lambda} = (\lambda_i)_{1 \leq i \leq I+J} \in \mathbb{R}^{I+J}$ represents the penalty parameters that control the tradeoff between satisfying the constraints and optimizing the cost. Note that the penalty for violations of the constraints becomes more significant as $\boldsymbol{\lambda}$ increases. Following UL-based solvers (Wang et al., 2022; Schuetz et al., 2022a; Karalias & Loukas, 2020), our study focuses on solving constrained CO problems using the penalty method. In the following, we briefly describe specific CO problems. Refer to Appendix D.1 for the underlying theoretical background of the following problems.

Example 1: MIS Problem. The MIS problem is a fundamental NP-hard problem (Karp, 2010) that has various practical applications in the network design (Hale, 1980) and finance (Boginski et al., 2005) fields. The MIS problem is defined as follows. Given an undirected graph $G(V, E)$, where V is the set of nodes with cardinality $|V| = N$, and $E \subseteq V \times V$ is the set of edges, an independent set (IS) is a subset of nodes $\mathcal{I} \in V$ where any two nodes in the set are not adjacent. The MIS problem attempts to find the largest IS, which is denoted \mathcal{I}^* . In this study, ρ denotes the IS density, where $\rho = |\mathcal{I}|/|V|$. To formulate the problem, a binary variable x_i is assigned to each node $i \in V$. The MIS problem, which is identical to maximizing the number of nodes assigned 1 while ensuring that these nodes are not adjacent, is formulated as follows:

$$f(\mathbf{x}; G, \lambda) = - \sum_{i \in V} x_i + \lambda \sum_{(i,j) \in E} x_i x_j, \quad (3)$$

where the first term attempts to maximize the number of nodes assigned 1, and the second term penalizes the adjacent nodes marked 1 according to the penalty parameter λ .

Example 2: MaxCut Problem. The MaxCut problem is also a fundamental NP-hard problem (Karp, 2010) with practical application in machine scheduling (Alidaee et al., 1994), image recognition (Neven et al., 2008) and electronic circuit layout design (Deza & Laurent, 1994). The MaxCut problem is defined as follows. Given an undirected graph $G = (V, E)$, a cut set $\mathcal{C} \in E$ is defined as a subset of the edge set between the node sets dividing $(V_1, V_2 \mid V_1 \cup V_2 = V, V_1 \cap V_2 = \emptyset)$. The MaxCut problems aim to find the maximum cut set, denoted \mathcal{C}^* . Here, the cut ratio is defined as $\nu = |\mathcal{C}|/|V|$, where $|\mathcal{C}|$ is the cardinality of the cut set. To formulate this problem, each node is assigned a binary variable, where $x_i = 1$ indicates that node i belongs to V_1 , and $x_i = 0$ indicates that the node belongs to V_2 . Here, $x_i + x_j - 2x_i x_j = 1$ holds if the edge $(i, j) \in \mathcal{C}$; otherwise, this is equal to 0. As a result, we obtain the following:

$$f(\mathbf{x}; G) = \sum_{i < j} A_{ij} (2x_i x_j - x_i - x_j) \quad (4)$$

where A_{ij} is the adjacency matrix with $A_{ij} = 0$ if an edge (i, j) does not exist and $A_{ij} > 0$ if the edge connects.

LCO. LCO problems involve leaning an algorithm $\mathcal{A}_\theta(\cdot) : \mathcal{C} \rightarrow \{0, 1\}^N$ parameterized by a nural network (NN), where θ denotes the parameters. Given an instance parameter $C \in \mathcal{C}$, this algorithm generates a valid solution $\hat{\mathbf{x}} = \mathcal{A}_\theta(C) \in \mathcal{X}(C)$ and minimizes $f(\hat{\mathbf{x}}; C)$. Several approaches have been proposed to learn \mathcal{A}_θ . This study focuses on UL-based solvers, where no labeled solution $\mathbf{x}^* \in \operatorname{argmin}_{\mathbf{x} \in \mathcal{X}(C)} f(\mathbf{x}; C)$ is employed during training (Wang et al., 2022; Schuetz et al., 2022a; Karalias & Loukas, 2020; Amizadeh et al., 2018).

Continuous Relaxation and UL-based Solver. The continuous relaxation strategy involves reformulating an original CO problem into a continuous optimization problem by converting discrete variables into continuous variables. A typical example of continuous relaxation can be expressed as follows:

$$\min_{\mathbf{p}} \hat{l}(\mathbf{p}; C, \lambda), \quad \hat{l}(\mathbf{p}; C, \lambda) \triangleq \hat{f}(\mathbf{p}; C) + \sum_{i=1}^{m+p} \lambda_i \hat{v}_i(\mathbf{p}; C),$$

where $\mathbf{p} = (p_i)_{1 \leq i \leq N} \in [0, 1]^N$ represents a set of relaxed continuous variables, i.e., each binary variable $x_i \in \{0, 1\}$ is relaxed to a continuous one $p_i \in [0, 1]$, and $\hat{f} : [0, 1]^N \times \mathcal{C} \rightarrow \mathbb{R}$ is the relaxation of f , satisfying $\hat{f}(\mathbf{x}; C) = f(\mathbf{x}; C)$ for $\mathbf{x} \in \{0, 1\}^N$. The relation between the constraint v_i and its relaxation \hat{v}_i is similar for $i \in [I + J]$, i.e., $\forall i \in [I + J], \hat{v}_i(\mathbf{x}; C) = v_i(\mathbf{x}; C)$ for $\mathbf{x} \in \{0, 1\}^N$.

Wang et al. (2022) and Schuetz et al. (2022a) formulated $\mathcal{A}_\theta(C)$ as the relaxed continuous variables, i.e., $\mathcal{A}_\theta(\cdot) : \mathcal{C} \rightarrow [0, 1]^n$. In the following discussions, to represent the parametrization of the relaxed variables explicitly, we denote \mathcal{A}_θ by \mathbf{p}_θ . Then, \mathbf{p}_θ is optimized by minimizing the following function directly:

$$\hat{l}(\theta; C, \lambda) \triangleq \hat{f}(\mathbf{p}_\theta(C); C) + \sum_{i=1}^{I+J} \lambda_i \hat{v}_i(\mathbf{p}_\theta(C); C). \quad (5)$$

The PI-GNN solver (Schuetz et al., 2022a;b) studies CO problems on graphs, i.e., $C = G(V, E)$, and employs GNNs for the relaxed vector $\mathbf{p}_\theta(G)$. Here, an L -layered GNN is trained to directly minimize $\hat{l}(\theta; C, \lambda)$ in Eq. (5), taking as input a graph G and the embedding vectors on the nodes, i.e., $\mathbf{h}^{(0)} \in \mathbb{R}^{H^{(0)}}$, and outputting the relaxed solution $\mathbf{h}^{(L)} = \mathbf{p}_\theta(G) \in [0, 1]^N$. A detailed description of the GNN is given in Appendix D.2. Thus, this approach is applicable to the cost functions with the following property due to the use of a gradient-based algorithm to minimize Eq (5).

Assumption 1.1 (Differentiable cost function). The relaxed cost function $\hat{l}(\theta; C)$ and its partial derivative $\partial \hat{l} / \partial \theta$ are accessible during the optimization process.

These properties involve nonlinear cost function and many-body interactions beyond just two-body interactions. After training the \mathbf{p}_θ , the relaxed solution is transformed into discrete variables simply by rounding \mathbf{p}_θ such as $\forall i \in [N], x_i = \operatorname{int}(p_{\theta,i}(C))$ with a threshold (Schuetz et al., 2022a), greedy method (Wang et al., 2022), or sampling from Bernoulli distribution with the parameter \mathbf{p}_θ such as $\forall i \in [N], x_i \sim \operatorname{Bernouli}(p_{\theta,i}(C))$.

2. Continuous Relaxation Annealing for UL-based Solver

In this section, we initially discuss the practical issues of UL-based solvers, and then introduce continuous relaxation annealing (CRA) by addressing these issues.

2.1. Motivation: Practical Issues of UL-based Solver

The practical application of UL-based solvers involves the following fundamental issues.

Ambiguity for Rounding Method After Learning UL-based solvers inherently face ambiguity when employing a continuous relaxation strategy. This strategy results in a potential disagreement between the optimal solutions of the original discrete CO problem and those of the relaxed continuous ones because the relaxation expands the solution space, which frequently leads to deviations from the binary values. Thus, UL-based solvers adopt artificial rounding methods back into the original discrete space. However, some relaxed problems exhibit half-integrality, where optimal solutions of the relaxed problems includes half-integral variables, $1/2$ (Nemhauser & Trotter Jr, 1974). Therefore, the results may vary depending on the selected rounding method, thereby potentially undermining solution robustness.

Difficulty of Optimizing Learnable Parameters Recently, Angelini & Ricci-Tersenghi (2023) demonstrated that the PI-GNN solver does not achieve results that are comparable to those of the degree-based greedy algorithm (Angelini & Ricci-Tersenghi, 2019) in the MIS problems on RRGs. In addition, the importance of evaluating UL-based solvers in complex CO problems, where the performance of greedy algorithms worsens, has been emphasized (Angelini & Ricci-Tersenghi, 2023). The representative example is MIS problems on RRGs with a constant degree $d > 16$, where a clustering transition occurs in the solution space, and the clusters form barriers, thereby affecting optimization. Moreover, Wang & Li (2023) pointed out that the PI-GNN solver tends to be trapped in local optimum because it is directly optimized for each instance without using historical data.

Therefore, we conducted numerical experiments using the PI-GNN solver for MIS and MaxCut problems on RRGs with higher degrees. To ensure the experimental impartiality, we adhered to the original settings of the PI-GNN solver (Schuetz et al., 2022b). Refer to Section 3.1 for the detailed experimental settings. Figure 1 (top) shows the solutions obtained by the PI-GNN solver as a function of the degree d for the MIS and MaxCut problems with varying system sizes N . These results indicate that finding independent and cut sets becomes unfeasible as the RRG becomes denser. In addition, to clarify the reasons for these failures, we ana-

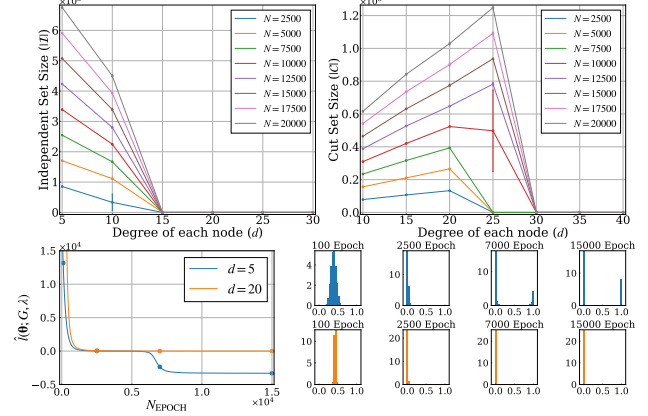


Figure 1. The top graph shows the independent set density for MIS problems (left) and the cut ratio for MaxCut problems (right) as a function of degree d using the PI-GNN solver with varying system size N . Each data point represents the average result of five different graph instances, with the error bars indicating the standard deviation of those results. The bottom graph shows the cost as a function of the number of parameter updates N_{EPOCH} , for $N = 10000$ MIS problems on 5-RRG and 20-RRG. The histogram represents the relaxed vector distribution with varying numbers of parameter updates N_{EPOCH} . Each point in the bottom-left plot is linked to the corresponding bottom-right histogram.

lyzed the dynamics of the cost function for MIS problems with $N = 10,000$, with a specific focus on a graph with degrees $d = 5$ and $d = 20$, as depicted in Figure 1 (bottom). For the $d = 5$ case, the cost function goes over the plateau of $\hat{l}(\theta; G, \lambda) = 0$ with $p_\theta(G) = \mathbf{0}_N$, as investigated in the histogram, eventually yielding a solution comparable to those presented by Schuetz et al. (2022a). Conversely, in the $d = 20$ case, the cost function remains stagnant on the plateau of $\hat{l}(\theta; G, \lambda) = 0$ with $p_\theta(G) = \mathbf{0}_N$, thereby failing to find any independent nodes. Interpreting this phenomenon, we hypothesize that the representation capacity of the GNN is sufficiently large, leading us to consider the optimization of $\hat{L}_{\text{MIS}}(\theta; G, \lambda)$ and $\hat{L}_{\text{MaxCut}}(\theta; G)$ as a variational optimization problem relative to p_θ . In this case, $p_\theta^* = \mathbf{0}_N$ satisfies the first-order variational optimality conditions $\delta\hat{l}_{\text{MIS}}/\delta p_\theta|_{p_\theta=p^*} = \delta\hat{l}_{\text{MaxCut}}/\delta p_\theta|_{p_\theta=p^*} = \mathbf{0}_N$, which implies a potential reason for absorption into the plateau. However, this does not reveal the conditions for the convergence to the fixed point p^* during the early learning stage or the condition to escape from the fixed point p^* . Thus, an extensive theoretical evaluation through stability analysis remains an important topic for future work.

2.2. Continuous Relaxation Annealing

Penalty Term to Control Discreteness and Continuity. To address these issues, we propose a penalty term to control

the discreteness and continuity of the relaxed variables. The proposed penalty term is expressed as follows:

$$\begin{aligned}\hat{r}(\mathbf{p}; C, \boldsymbol{\lambda}, \gamma) &= \hat{l}(\mathbf{p}; C, \boldsymbol{\lambda}) + \Phi(\mathbf{p}; C, \gamma, \alpha), \\ \Phi(\mathbf{p}; C, \gamma, \alpha) &\triangleq \gamma \sum_{i=1}^N (1 - (2p_i - 1)^\alpha)\end{aligned}\quad (6)$$

where $\gamma \in \mathbb{R}$ represents a penalty parameter. For a negative γ value, i.e., $\gamma < 0$, the relaxed variables tend to favor the continuous space. In contrast, for a positive γ value, i.e., $\gamma > 0$, the relaxed variables prefer discrete space. In addition, as λ approaches $\pm\infty$, the following theorem holds.

Theorem 2.1. *Under the assumption that the objective function $\hat{l}(\mathbf{p}; C)$ is bounded within the domain $[0, 1]^N$, as $\gamma \rightarrow +\infty$, the soft solutions $\mathbf{p}^* \in \operatorname{argmin}_{\mathbf{p}} \hat{r}(\mathbf{p}; C, \boldsymbol{\lambda}, \gamma)$ converge to the original solutions $\mathbf{x}^* \in \operatorname{argmin}_{\mathbf{x}} l(\mathbf{x}; C, \boldsymbol{\lambda})$. In addition, as $\gamma \rightarrow -\infty$, the loss function $\hat{r}(\mathbf{p}; C, \boldsymbol{\lambda}, \gamma)$ becomes convex, and the soft solution $\mathbf{1}_N/2 = \operatorname{argmin}_{\mathbf{p}} \hat{r}(\mathbf{p}; C, \boldsymbol{\lambda}, \gamma)$ is unique.*

Refer to Appendix B.1 for the detailed proof. In addition, the penalty term eliminates the stationary point $\mathbf{p}^* = \mathbf{0}_n$ in Section 2.1, which leads to avoiding convergence to the plateau. For UL-based solvers, the penalty term is expressed as follows:

$$\hat{r}(\boldsymbol{\theta}; C, \boldsymbol{\lambda}, \gamma) = \hat{l}(\boldsymbol{\theta}; C, \boldsymbol{\lambda}) + \Phi(\boldsymbol{\theta}; C, \gamma, \alpha), \quad (7)$$

where $\Phi(\boldsymbol{\theta}; C, \gamma, \alpha) \triangleq \Phi(\mathbf{p}_\theta(C); C, \gamma, \alpha)$. From Theorem 2.1, the relaxed variables approach nearly discrete variables by setting a sufficiently large γ value.

Annealing Penalty Term. We propose an annealing strategy that gradually anneals the penalty parameter γ in Eq. (7). First, we set a negative gamma value, i.e., $\gamma < 0$, to leverage the properties that eliminate the fixed point $\mathbf{p}^* = \mathbf{0}_N$ and to facilitate extensive exploration via convexity of $\Phi(\boldsymbol{\theta}; C, \gamma, \alpha)$ during the early learning stage. Then, we increase the penalty parameter γ gradually at each update of the trainable parameters, denoted as 1 epoch, until the penalty term is nearly zero, i.e., $\Phi(\boldsymbol{\theta}, C, \gamma, \alpha) \approx 0$. This indicates that the relaxed variables \mathbf{p}_θ are nearly discrete. Therefore, we also propose an early stopping strategy that monitors the loss function and the penalty term $\Phi(\boldsymbol{\theta}; C, \gamma, \alpha)$ in Eq. (7) to stop the annealing and learning processes when the penalty term approaches zero, i.e., $\Phi(\boldsymbol{\theta}, C) \approx 0$. Note that various annealing schedules can be considered for such cases; however, the current study employs the following scheduling strategy, $\gamma(N_{\text{EPOCH}} + 1) \leftarrow \gamma(N_{\text{EPOCH}}) + \varepsilon$, where the scheduling rate $\varepsilon \in \mathbb{R}$ is a small constant value, and N_{EPOCH} is the number of updates of the trainable parameter during the learning process. In the following, we refer to the PI-GNN solver with this annealing as the CRA-PI-GNN solver. Here, two additional hyperparameters are introduced, i.e., the initial scheduling value

$\gamma(0)$ and the scheduling rate ε . The results of our numerical experiment suggest that better solutions can be obtained when the initial scheduling value $\gamma(0)$ has a small negative value and the scheduling rate ε is small.

3. Experiments

In this section, we first analyze the performance of the CRA-PI-GNN solver for the MaxCut and MIS benchmark problems on multiple graphs with different numbers of nodes. Then, we show the results for the DBM problems as an example of more practical CO problems.

3.1. Experimental Settings

Baseline Methods. In all experiments, the baseline methods include the PI-GNN solver (Schuetz et al., 2022a) as the direct baseline. For the MIS problems, we also consider the random greedy algorithm (RGA) and DGA (Angelini & Ricci-Tersenghi, 2019) as heuristic baselines. For the MaxCut problems, the RUN-CSP solver (Toenshoff et al., 2019) is considered as an additional baseline. Note that we do not consider UL-based solvers that utilize historical data (Karalias & Loukas, 2020; Wang & Li, 2023) because the goal of this study is to determine whether the CRA-PI-GNN solver, which optimizes each instance directly, can outperform the PI-GNN solver and greedy algorithms.

Implementation The main objective of these numerical experiments is to compare the CRA-PI-GNN solver with the PI-GNN solver. Thus, we follow the experimental configuration described in the literature (Schuetz et al., 2022a; 2023), employing a simple two-layer GCV and GraphSAGE (Hamilton et al., 2017) architecture with PyTorch GraphConv and GraphSage implemented using the Deep Graph Library (Wang et al., 2019). Here, the first convolutional layer takes $H^{(0)}$ -dimensional node embedding vectors, $\mathbf{h}_\theta^{(0)}$ for each node, as input, yielding $H^{(1)}$ -dimensional feature vectors $\mathbf{h}_\theta^{(1)}$. Then, the ReLU function is applied as a component-wise nonlinear transformation. The second convolutional layer takes the $H^{(1)}$ -dimensional feature vectors, $\mathbf{h}_\theta^{(1)}$, as input, producing a $H^{(2)}$ -dimensional vector $\mathbf{h}_\theta^{(2)}$. Finally, a sigmoid function is applied to the $H^{(2)}$ -dimensional vector $\mathbf{h}_\theta^{(2)}$, and the output is the soft solution $\mathbf{p}_\theta \in [0, 1]^N$. As in (Schuetz et al., 2022a), we set $H^{(0)} = \text{int}(N^{0.8})$ or, $H^{(1)} = \text{int}(N^{0.8}/2)$ and $H^{(2)} = 1$ for both GCN and GraphSAGE. Here, we use the AdamW (Kingma & Ba, 2014) optimizer with a learning rate of $\eta = 10^{-4}$ and weight decay of 10^{-2} , and we train the GNNs for up to 10^5 epochs with early stopping set to the absolute tolerance 10^{-5} and patience 10^3 . As discussed in Schuetz et al. (2022a), the GNNs are initialized with five different random seeds for a single instance because the

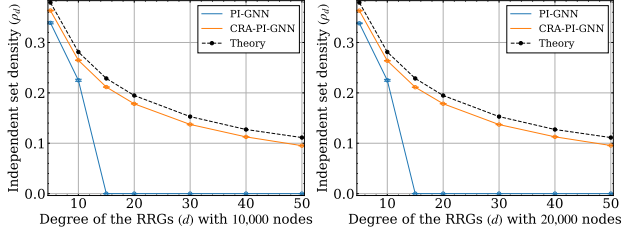


Figure 2. Independent set density of the MIS problem on d -RRG using the PI-GNN and CRA-PI-GNN solvers. (Left) Results for graphs with $N = 10,000$ nodes. (Right) Results for graphs with $N = 20,000$ nodes. Each data point illustrate the average results from five different graph instances. The error bars indicate the standard deviation. Various colors correspond to the solvers used, and the dashed lines represent the theoretical results obtained from a statistical mechanical analysis (Barbier et al., 2013).

results are dependent on the initial values of the trainable parameters; thus selecting the best solution. We set the initial scheduling value to $\gamma(0) = -20$ for the MIS and matching problems, and we set $\gamma(0) = -6$ for the MaxCut problems with the scheduling rate $\varepsilon = 10^{-3}$ and curve rate $\alpha = 2$ in Eq. (7). Note that these values are not necessarily optimal, and refining these parameter values can allow the CRA-PI-GNN solver to find better solutions. Refer to Appendix E.1 and Appendix E.2 for an ablation study of these hyperparameters. Once the training process is complete, we apply projection heuristics to map the obtained soft solutions back to discrete solutions using simple projection, where for all $i \in [N]$, we map $p_{\theta,i}$ into 0 if $p_{\theta,i} \leq 0.5$ and $p_{\theta,i}$ into 1 if $p_{\theta,i} > 0.5$. Due to the early stopping (Section 2.2), the CRA-PI-GNN solver ensures that for all benchmark CO problems, the soft solution at the end of the training process is nearly binary; thus, it is robust against a given threshold, which we set to 0.5 in our experiments.

Evaluation Metrics Following the metric of Wang & Li (2023), we use the approximation rate (ApR) for the MIS problems, formulated as $\text{ApR} = f(\mathbf{x}; C)/f(\mathbf{x}^*)$, where \mathbf{x}^* represents the theoretical results (Barbier et al., 2013). Additionally, we evaluate the independent set density ρ relative to the theoretical results. For the MaxCut problems on RRGs, we adopt the cut ratio ν against the theoretical upper bound (Parisi, 1980; Dembo et al., 2017). All the results for the MIS and MaxCut problems are summarized based on 5 RRGs with different random seeds. In the case of the MaxCut Gset problem, the ApR is calculated compared to the known best results. Regarding the DBM problems, we calculate the ApR against the global optimal, identified using Gurobi 10.0.1 solver with default settings.

3.2. MIS Problems

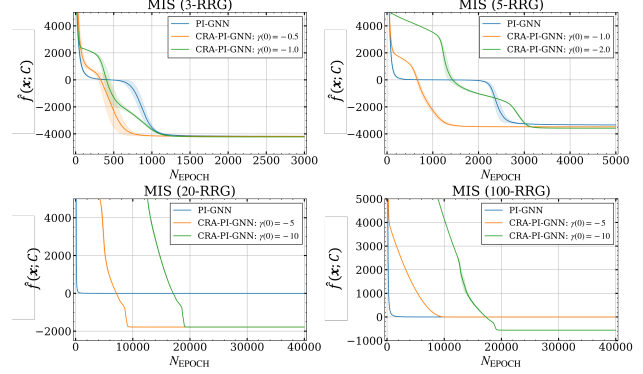


Figure 3. Cost function of $N = 10,000$ MIS problems on RRGs of varying degrees d as a function of the number of parameters updates N_{EPOCH} . The lines represent the average cost function over five different instances, and the shade corresponding to each line represents the standard deviation of the results.

Degree Dependency of Obtained Solutions. First, we compare the performance of the PI-GNN and CRA-PI-GNN solvers using GCV, as in Schuetz et al. (2022a). Figure 2 shows the independent set density ρ_d as a function of degree d obtained by the PI-GNN and CRA-PI-GNN solvers compared with the theoretical results (Barbier et al., 2013). When setting $\lambda = 2$, we observed zero violated nodes, as described in Schuetz et al. (2022a). Across all degrees d , the CRA-PI-GNN solver outperformed the PI-GNN solver and approached the reported theoretical results. In particular, the CRA-PI-GNN solver can find valid solutions even with an increasing degree d , whereas the PI-GNN solver fail to find valid solutions, especially for $d \geq 15$.

Response to Angelini & Ricci-Tersenghi (2023) and Wang & Li (2023). For the MIS problem on RRGs with a high node degree, e.g., $d = 20, 100$, Angelini & Ricci-Tersenghi (2019) recently raised concerns by arguing that the PI-GNN solver fails to achieve results that are comparable to those of the heuristic DGA (Angelini & Ricci-Tersenghi, 2019). In addition, Wang & Li (2023) have indicated that UL-based solvers, trained directly on a single instance without leveraging historical data, are likely to get trapped in local optima and fail to produce a valid solution. For these issues, the results shown in Table 1 demonstrate that the CRA-PI-GNN solver, which optimizes each instance directly without any history, can further improve the RGA (Angelini & Ricci-Tersenghi, 2019) and DGA (Angelini & Ricci-Tersenghi, 2019), while the PI-GNN solver the DGA and RGA.

Acceleration of Convergence Speed. We also compared the convergence speed of the cost functions between PI-GNN and CRA-PI-GNN solver and confirmed that the CRA-

Table 1. ApR in MIS problems on RRGs with 10,000 nodes and node degree $d = 20, 100$. ‘‘CRA’’ represents the CRA-PI-GNN solver.

GRAPH	RGA	DGA	PI-GNN (GCV)	PI-GNN (SAGE)	CRA (GCV)	CRA (SAGE)
20-RRG	0.776 ± 0.001	0.891 ± 0.001	0.000 ± 0.000	0.745 ± 0.003	0.937 ± 0.002	0.963 ± 0.001
100-RRG	0.663 ± 0.001	0.848 ± 0.002	0.000 ± 0.000	0.000 ± 0.000	0.855 ± 0.004	0.924 ± 0.001

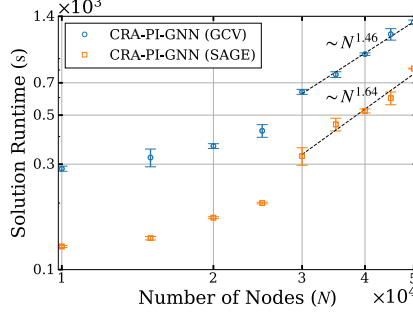


Figure 4. (Right) computational runtime (in seconds) of the CRA-PI-GNN solvers with the GraphSage and Conv architectures on 100-RRG with varying numbers of nodes N . Error bars represent the standard deviations of the results.

PI-GNN solver does not become trapped in the plateau, as discussed in Section 2.1. Figure 3 shows the epoch dependence of the cost functions for each solver for the MIS problems with $N = 10,000$ across $d = 3, 5, 20, 100$. Across all degrees, the CRA-PI-GNN solver effectively escapes the plateau, where all variables are zero, which allows it to obtain a better solution with fewer epochs than the PI-GNN solver.

Computational Scaling As reported in the literature (Schuetz et al., 2022a; Wang & Li, 2023), we also evaluate the computational scaling of the CRA-PI-GNN solver for MIS problems with large-scale RRGs with a node degree of 100. As shown in Figure 4, we can observe a moderate super-linear scaling of the total computational time, approximately $\sim N^{1.4}$ for GCN and $\sim N^{1.7}$ for GraphSage. This performance is nearly identical to that of the PI-GNN solver (Schuetz et al., 2022a) for problems on RRGs with lower degrees.

3.3. MaxCut Problem

Degree Dependency of Obtained Solutions. First, following Schuetz et al. (2022a), we compare the performances of the PI-GNN and CRA-PI-GNN solvers with GCV. Figure 5 shows the cut ratio ν_d as a function of the degree d compared to the theoretical upper bound (Parisi, 1980; Dembo et al., 2017). Across all degrees d , the CRA-PI-GNN solver approaches the theoretical upper bound and outperforms the PI-GNN solver, which struggles to find a cut set for $d > 20$.

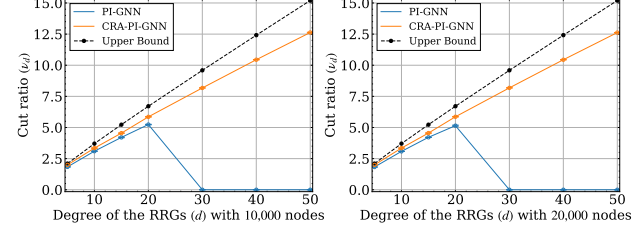


Figure 5. Cut ratio of the MaxCut problem on d -RRG as a function of the degree d using the PI-GNN and CRA-PI-GNN solvers. (Left) Results for $N = 10,000$. (Right) Results for $N = 20,000$ bits. Each data point represents the average results over five different graph instances, with the error bars indicating the standard deviations. The different colors represent the compared solvers, and the dashed lines represent the theoretical upper bounds.

Table 2. ApR for MaxCut on Gset

(NODES, EDGES)	RUN-CSP	PI-GNN	CRA
G14 (800, 4,694)	0.960	0.988	0.994
G15 (800, 4,661)	0.960	0.980	0.992
G22 (2,000, 19,990)	0.975	0.987	0.998
G49 (3,000, 6,000)	1.000	0.986	1.000
G50 (3,000, 6,000)	1.000	0.990	1.000
G55 (5,000, 12,468)	0.982	0.983	0.991
G70 (10,000, 9,999)	—	0.982	0.992

Standard MaxCut Benchmark Test. As discussed by Schuetz et al. (2022a), we conducted additional experiments on standard MaxCut benchmark instances based on the publicly available Gset dataset (Ye, 2003), which is commonly used to evaluate MaxCut algorithms. Here, we provide benchmark results for seven distinct graphs with thousands of nodes, including Erdős-Renyi graphs with uniform edge probability, graphs in which the connectivity decays gradually from node 1 to N , 4-regular toroidal graphs, and a very large Gset instance with $N = 10,000$ nodes. The corresponding results are shown in Table 2. As can be seen, across all problems, the CRA-PI-GNN solver outperforms both the PI-GNN and RUN-CSP solvers.

3.4. Diverse Bipartite Matching

To evaluate the applicability of the CRA-PI-GNN solver to more practical problems, we conducted experiments on

diverse bipartite matching problems (Ferber et al., 2020; Mulamba et al., 2020; Mandi et al., 2022). Here, the topologies are taken from the Cora citation network (Sen et al., 2008), where each node has 1,433 bag-of-words features, and each edge represents likelihood, as predicted by a machine learning model. Mandi et al. (2022) focused on disjoint topologies within the given topology, and they created 27 distinct instances with varying properties. Each instance comprises 100 nodes representing scientific publications, divided into two groups of 50 nodes N_1 and N_2 . The optimization task is to find the maximum matching, where diversity constraints ensure connections among papers in the same field and between papers of different fields. This is formulated using a penalty method as follows.

$$\begin{aligned} l(\mathbf{x}; C, M, \boldsymbol{\lambda}) = & - \sum_{ij} C_{ij} x_{ij} \\ & + \lambda_1 \sum_i \text{ReLU} \left(\sum_j x_{ij} - 1 \right) \\ & + \lambda_2 \sum_j \text{ReLU} \left(\sum_i x_{ij} - 1 \right) \\ & + \lambda_3 \text{ReLU} \left(p \sum_{ij} x_{ij} - \sum_{ij} M_{ij} x_{ij} \right) \\ & + \lambda_4 \text{ReLU} \left(q \sum_{ij} x_{ij} - \sum_{ij} (1 - M_{ij}) x_{ij} \right), \end{aligned} \quad (8)$$

where $C \in \mathbb{R}^{N_1 \times N_2}$ represents the likelihood of a link between each pair of nodes, an indicator M_{ij} is set to 0 if article i and j share the same subject field (1 otherwise) $\forall i \in N_1$, and $j \in N_2$. The parameters $p, q \in [0, 1]$ represent the probability of pairs sharing their field and of unrelated pairs, respectively. As in Mandi et al. (2022), we explore two variations of this problem, with $p = q =$ being 25% and 5%, respectively, and these variations are referred to as Matching-1 and Matching-2, respectively. In this experiment, we set $\lambda_1 = \lambda_2 = 10$ and $\lambda_3 = \lambda_4 = 25$. Figure 6 shows that the CRA-PI-GNN solver can find better solutions across all instances.

4. Related Work

Previous studies on UL-based solvers have investigated constraint satisfaction problems (Toenshoff et al., 2019; Amizadeh et al., 2018) and traveling salesman problems (Hudson et al., 2021) using carefully designed cost functions specific to these problems. However, employing these approaches to address general CO problems requires problem reductions. To optimize general CO problems directly, Karalias & Loukas (2020) proposed a UL-based solver using Erdős' probabilistic method, which associates the output of the NN with probability. Subsequently, Wang et al. (2022) generalized this UL-solver and demonstrated that a high-quality solution can be obtained if the CO cost function can be relaxed into an entry-wise concave form. Recently, Schuetz et al. (2022a;b) extended this UL-based solver (Karalias & Loukas, 2020) to large-scale CO problems. In addition, Wang & Li (2023) indicated that UL-based solvers

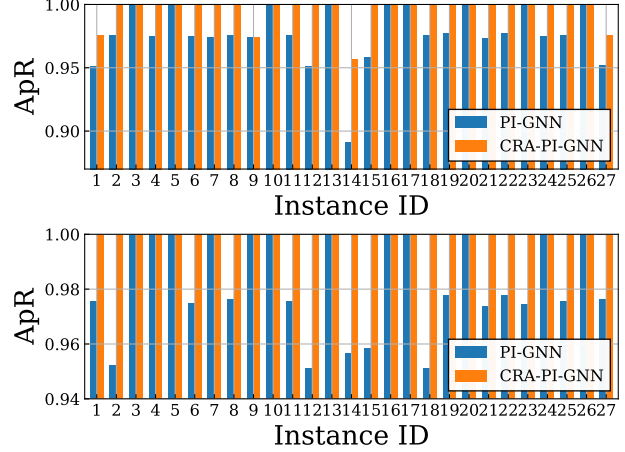


Figure 6. ApR on diverse bipartite matching problems.

optimized over each instance tend to become trapped in a local optimum, and they pointed out the importance of learning from historical instances. To address this issue, Wang & Li (2023) applied meta-learning to a UL-based solver using historical instances. However, the CRA-PI-GNN solver outperformed greedy algorithms without historical instances.

5. Conclusion

This study addresses two practical issues of UL-based solvers: the ambiguity in rounding caused by the continuous relaxation strategy and the difficulty of optimizing learnable parameters due to local optima by applying the CRA to the PI-GNN solvers. The CRA introduces a penalty term to regulate the discreteness and continuity of the relaxed variables and eliminate local optima. Additionally, the CRA involves an annealing process for the penalty term, initially prioritizing continuous solutions and progressively transitioning towards discrete solutions until the relaxed variables become nearly discrete, eliminating the artificial rounding. Our experiments demonstrate that the CRA-PI-GNN solver, which directly optimizes each instance without any history, significantly outperforms the PI-GNN solvers, other state-of-the-art UL-based baseline methods, and greedy algorithms. Moreover, the CRA-PI-GNN solver can find better solutions faster than the PI-GNN solver by effectively eliminating the local optimal. These results address previous concerns regarding the potential underperformance of the PI-GNN solvers to greedy algorithms when historical data is unavailable, offering promising directions for future development. However, a limitation of UL-based solvers is the considerable time required for tuning penalty parameters, a critical issue that needs addressing.

References

Alidaee, B., Kochenberger, G. A., and Ahmadian, A. 0-1 quadratic programming approach for optimum solutions of two scheduling problems. *International Journal of Systems Science*, 25(2):401–408, 1994.

Amizadeh, S., Matusevych, S., and Weimer, M. Learning to solve circuit-sat: An unsupervised differentiable approach. In *International Conference on Learning Representations*, 2018.

Angelini, M. C. and Ricci-Tersenghi, F. Monte carlo algorithms are very effective in finding the largest independent set in sparse random graphs. *Physical Review E*, 100(1):013302, 2019.

Angelini, M. C. and Ricci-Tersenghi, F. Modern graph neural networks do worse than classical greedy algorithms in solving combinatorial optimization problems like maximum independent set. *Nature Machine Intelligence*, 5(1):29–31, 2023.

Anthony, M., Boros, E., Crama, Y., and Gruber, A. Quadratic reformulations of nonlinear binary optimization problems. *Mathematical Programming*, 162:115–144, 2017.

Barbier, J., Krzakala, F., Zdeborová, L., and Zhang, P. The hard-core model on random graphs revisited. In *Journal of Physics: Conference Series*, volume 473, pp. 012021. IOP Publishing, 2013.

Bayati, M., Gamarnik, D., and Tetali, P. Combinatorial approach to the interpolation method and scaling limits in sparse random graphs. In *Proceedings of the forty-second ACM symposium on Theory of computing*, pp. 105–114, 2010.

Bello, I., Pham, H., Le, Q. V., Norouzi, M., and Bengio, S. Neural combinatorial optimization with reinforcement learning. *arXiv preprint arXiv:1611.09940*, 2016.

Boginski, V., Butenko, S., and Pardalos, P. M. Statistical analysis of financial networks. *Computational statistics & data analysis*, 48(2):431–443, 2005.

Chen, X. and Tian, Y. Learning to perform local rewriting for combinatorial optimization. *Advances in Neural Information Processing Systems*, 32, 2019.

Coja-Oghlan, A. and Efthymiou, C. On independent sets in random graphs. *Random Structures & Algorithms*, 47(3):436–486, 2015.

Dembo, A., Montanari, A., and Sen, S. Extremal cuts of sparse random graphs. 2017.

Deza, M. and Laurent, M. Applications of cut polyhedra—ii. *Journal of Computational and Applied Mathematics*, 55(2):217–247, 1994.

Ferber, A., Wilder, B., Dilkina, B., and Tambe, M. Mipaal: Mixed integer program as a layer. In *Proceedings of the AAAI Conference on Artificial Intelligence*, volume 34, pp. 1504–1511, 2020.

Gasse, M., Chételat, D., Ferroni, N., Charlin, L., and Lodi, A. Exact combinatorial optimization with graph convolutional neural networks. *Advances in neural information processing systems*, 32, 2019.

Gilmer, J., Schoenholz, S. S., Riley, P. F., Vinyals, O., and Dahl, G. E. Neural message passing for quantum chemistry. In *International conference on machine learning*, pp. 1263–1272. PMLR, 2017.

Glover, F., Kochenberger, G., and Du, Y. Quantum bridge analytics i: a tutorial on formulating and using qubo models. *4or*, 17:335–371, 2019.

Hale, W. K. Frequency assignment: Theory and applications. *Proceedings of the IEEE*, 68(12):1497–1514, 1980.

Hamilton, W., Ying, Z., and Leskovec, J. Inductive representation learning on large graphs. *Advances in neural information processing systems*, 30, 2017.

Hoffman, A. J. and Kruskal, J. B. Integral boundary points of convex polyhedra. *50 Years of Integer Programming 1958-2008: From the Early Years to the State-of-the-Art*, pp. 49–76, 2010.

Hudson, B., Li, Q., Malencia, M., and Prorok, A. Graph neural network guided local search for the traveling salesperson problem. *arXiv preprint arXiv:2110.05291*, 2021.

Joshi, C. K., Laurent, T., and Bresson, X. An efficient graph convolutional network technique for the travelling salesman problem. *arXiv preprint arXiv:1906.01227*, 2019.

Karalias, N. and Loukas, A. Erdos goes neural: an unsupervised learning framework for combinatorial optimization on graphs. *Advances in Neural Information Processing Systems*, 33:6659–6672, 2020.

Karp, R. M. *Reducibility among combinatorial problems*. Springer, 2010.

Khalil, E., Le Bodic, P., Song, L., Nemhauser, G., and Dilkina, B. Learning to branch in mixed integer programming. In *Proceedings of the AAAI Conference on Artificial Intelligence*, volume 30, 2016.

Khalil, E., Dai, H., Zhang, Y., Dilksina, B., and Song, L. Learning combinatorial optimization algorithms over graphs. *Advances in neural information processing systems*, 30, 2017.

Kingma, D. P. and Ba, J. Adam: A method for stochastic optimization. *arXiv preprint arXiv:1412.6980*, 2014.

Kochenberger, G., Hao, J.-K., Glover, F., Lewis, M., Lü, Z., Wang, H., and Wang, Y. The unconstrained binary quadratic programming problem: a survey. *Journal of combinatorial optimization*, 28:58–81, 2014.

Kool, W., Van Hoof, H., and Welling, M. Attention, learn to solve routing problems! *arXiv preprint arXiv:1803.08475*, 2018.

Korte, B. H., Vygen, J., Korte, B., and Vygen, J. *Combinatorial optimization*, volume 1. Springer, 2011.

Kwon, Y.-D., Choo, J., Kim, B., Yoon, I., Gwon, Y., and Min, S. Pomo: Policy optimization with multiple optima for reinforcement learning. *Advances in Neural Information Processing Systems*, 33:21188–21198, 2020.

Mandi, J., Bucarey, V., Tchomba, M. M. K., and Guns, T. Decision-focused learning: through the lens of learning to rank. In *International Conference on Machine Learning*, pp. 14935–14947. PMLR, 2022.

Mazyavkina, N., Sviridov, S., Ivanov, S., and Burnaev, E. Reinforcement learning for combinatorial optimization: A survey. *Computers & Operations Research*, 134:105400, 2021.

Mnih, V., Kavukcuoglu, K., Silver, D., Rusu, A. A., Veness, J., Bellemare, M. G., Graves, A., Riedmiller, M., Fidjeland, A. K., Ostrovski, G., et al. Human-level control through deep reinforcement learning. *nature*, 518(7540):529–533, 2015.

Mulamba, M., Mandi, J., Diligenti, M., Lombardi, M., Bucarey, V., and Guns, T. Contrastive losses and solution caching for predict-and-optimize. *arXiv preprint arXiv:2011.05354*, 2020.

Nazari, M., Oroojlooy, A., Snyder, L., and Takáć, M. Reinforcement learning for solving the vehicle routing problem. *Advances in neural information processing systems*, 31, 2018.

Nemhauser, G. L. and Trotter Jr, L. E. Properties of vertex packing and independence system polyhedra. *Mathematical programming*, 6(1):48–61, 1974.

Neven, H., Rose, G., and Macready, W. G. Image recognition with an adiabatic quantum computer i. mapping to quadratic unconstrained binary optimization. *arXiv preprint arXiv:0804.4457*, 2008.

Papadimitriou, C. H. and Steiglitz, K. *Combinatorial optimization: algorithms and complexity*. Courier Corporation, 1998.

Parisi, G. A sequence of approximated solutions to the sk model for spin glasses. *Journal of Physics A: Mathematical and General*, 13(4):L115, 1980.

Scarselli, F., Gori, M., Tsoi, A. C., Hagenbuchner, M., and Monfardini, G. The graph neural network model. *IEEE transactions on neural networks*, 20(1):61–80, 2008.

Schuetz, M. J., Brubaker, J. K., and Katzgraber, H. G. Combinatorial optimization with physics-inspired graph neural networks. *Nature Machine Intelligence*, 4(4):367–377, 2022a.

Schuetz, M. J., Brubaker, J. K., Zhu, Z., and Katzgraber, H. G. Graph coloring with physics-inspired graph neural networks. *Physical Review Research*, 4(4):043131, 2022b.

Schuetz, M. J., Brubaker, J. K., and Katzgraber, H. G. Reply to: Modern graph neural networks do worse than classical greedy algorithms in solving combinatorial optimization problems like maximum independent set. *Nature Machine Intelligence*, 5(1):32–34, 2023.

Selsam, D., Lamm, M., Bünz, B., Liang, P., de Moura, L., and Dill, D. L. Learning a sat solver from single-bit supervision. *arXiv preprint arXiv:1802.03685*, 2018.

Sen, P., Namata, G., Bilgic, M., Getoor, L., Galligher, B., and Eliassi-Rad, T. Collective classification in network data. *AI magazine*, 29(3):93–93, 2008.

Smith, A. E., Coit, D. W., Baeck, T., Fogel, D., and Michalewicz, Z. Penalty functions. *Handbook of evolutionary computation*, 97(1):C5, 1997.

Toenshoff, J., Ritzert, M., Wolf, H., and Grohe, M. Run-csp: unsupervised learning of message passing networks for binary constraint satisfaction problems. *CoRR*, abs/1909.08387, 2019.

Wang, H. and Li, P. Unsupervised learning for combinatorial optimization needs meta-learning. *arXiv preprint arXiv:2301.03116*, 2023.

Wang, H. P., Wu, N., Yang, H., Hao, C., and Li, P. Unsupervised learning for combinatorial optimization with principled objective relaxation. *Advances in Neural Information Processing Systems*, 35:31444–31458, 2022.

Wang, M., Zheng, D., Ye, Z., Gan, Q., Li, M., Song, X., Zhou, J., Ma, C., Yu, L., Gai, Y., et al. Deep graph library: A graph-centric, highly-performant package for graph neural networks. *arXiv preprint arXiv:1909.01315*, 2019.

Yao, W., Bandeira, A. S., and Villar, S. Experimental performance of graph neural networks on random instances of max-cut. In *Wavelets and Sparsity XVIII*, volume 11138, pp. 242–251. SPIE, 2019.

Ye, Y. The gset dataset. <https://web.stanford.edu/~yyye/yyye/Gset/>, 2003.

Yehuda, G., Gabel, M., and Schuster, A. It’s not what machines can learn, it’s what we cannot teach. In *International conference on machine learning*, pp. 10831–10841. PMLR, 2020.

Yolcu, E. and Póczos, B. Learning local search heuristics for boolean satisfiability. *Advances in Neural Information Processing Systems*, 32, 2019.

A. Overview

This supplementary material provides extended explanations, implementation details, and additional results.

B. Derivation

B.1. Proof of Theorem 3.1

First, we present three lemmas, and then we demonstrate Theorem 3.1 based on these lemmas.

Lemma B.1. *For any even natural number $\alpha = 2, 4, \dots$, the function $\phi(p; \alpha) = 1 - (2p - 1)^\alpha$ defined on $[0, 1]$ achieves its maximum value of 1 when $p = 1/2$ and its minimum value of 0 when $p = 0$ or $p = 1$.*

Proof. The derivative of $\phi(p; \alpha)$ relative to p is $\phi'(p; \alpha) = -2\alpha(2p - 1)$, which is zero when $p = 1/2$. This is a point where the function is maximized because the second derivative $\phi''(p; \alpha) = -4\alpha \leq 0$. In addition, this function is concave and symmetric relative to $p = 1/2$ because α is an even natural number, i.e., $\phi(p; \alpha) = \phi(1 - p; \alpha)$, thereby achieving its minimum value of 0 when $p = 0$ or $p = 1$. \square

Lemma B.2. *For any even natural number $\alpha = 2, 4, \dots$, if $\lambda \rightarrow +\infty$, minimizing the penalty term $\Phi(\mathbf{p}; \gamma, \alpha) = \gamma \sum_{i=1}^N (1 - (2p_i - 1)^\alpha) = \gamma \sum_{i=1}^N \phi(p_i; \alpha)$ enforces that the components of \mathbf{p} must be either 0 or 1 and, if $\gamma \rightarrow -\infty$, the penalty term enforces $\mathbf{p} = \mathbf{1}_N/2$.*

Proof. From Lemma B1, as $\gamma \rightarrow +\infty$, the case where $\phi(p; \alpha)$ becomes minimal occurs when, for each i , $p_i = 0$ or $p_i = 1$. In addition, as $\gamma \rightarrow -\infty$, the case where $\phi(p; \alpha, \gamma)$ is minimized occurs when, for each i , p_i reaches its maximum value with $p_i = 1/2$. \square

Lemma B.3. *$\Phi(\mathbf{p}; \gamma, \alpha) = \gamma \sum_{i=1}^N (1 - (2p_i - 1)^\alpha) = \gamma \sum_{i=1}^N \phi(p_i; \alpha)$ is concave when λ is positive and is a convex function when λ is negative.*

Proof. Note that $\Phi(\mathbf{p}; \gamma, \alpha) = \gamma \sum_{i=1}^N \phi(p_i; \alpha) = \gamma \sum_{i=1}^N (1 - (2p_i - 1)^\alpha)$ is separable across its components p_i . Thus, it is sufficient to prove that each $\gamma\phi_i(p_i; \alpha)$ is concave or convex in p_i because the sum of the concave or convex functions is also concave (and vice versa). Therefore, we consider the second derivative of $\gamma\phi_i(p_i; \alpha)$ with respect to p_i :

$$\gamma \frac{d^2\phi_i(p_i; \alpha)}{dp_i^2} = -4\gamma\alpha$$

Here, if $\gamma > 0$, the second derivative is negative for all $p_i \in [0, 1]$, and this completes the proof that $\Phi(\mathbf{p}; \gamma, \alpha)$ is a concave function when γ is positive over the domain $\mathbf{p} \in [0, 1]^N$. \square

Theorem B.4. *Assume that the objective function $\hat{l}(\mathbf{p}; C)$ is bounded within the domain $[0, 1]^n$. As $\gamma \rightarrow +\infty$, the soft solutions, i.e., $\mathbf{p}^* \in \operatorname{argmin}_{\mathbf{p}} \hat{r}(\mathbf{p}; C, \boldsymbol{\lambda}, \gamma)$, converge to the original solutions $\mathbf{x}^* \in \operatorname{argmin}_{\mathbf{x}} l(\mathbf{x}; C, \boldsymbol{\lambda})$, and as $\gamma \rightarrow -\infty$, the loss function $\hat{r}(\mathbf{p}; C, \boldsymbol{\lambda}, \gamma)$ becomes convex, and the soft solution $\mathbf{1}_N/2 = \operatorname{argmin}_{\mathbf{p}} \hat{r}(\mathbf{p}, C, \boldsymbol{\lambda}, \gamma)$ is unique.*

Proof. As $\lambda \rightarrow +\infty$, the penalty term $\Phi(\mathbf{p}; \alpha)$ dominates the loss function $\hat{r}(\mathbf{p}; C, \boldsymbol{\lambda}, \gamma)$. According to Lemma B.2, this penalty term forces the optimal solution \mathbf{p}^* to have components p_i^* that are either 0 or 1 because any nonbinary value will result in an infinitely large penalty. This effectively restricts the feasible region to the vertices of the unit hypercube, which correspond to the binary vector in $\{0, 1\}^N$. Thus, as $\lambda \rightarrow \infty$, the solutions to the relaxed problem converge to those of the original combinatorial problem. As $\lambda \rightarrow -\infty$, the penalty term $\Phi(\mathbf{p}; \alpha)$ also dominates the loss function $\hat{r}(\mathbf{p}; C, \boldsymbol{\lambda}, \gamma)$ and the $\hat{r}(\mathbf{p}; C, \boldsymbol{\lambda})$ convex function from Lemma B.3. According to Lemma B.2, this penalty term forces the optimal solution $\mathbf{p}^* = \mathbf{1}_N/2$. \square

C. Additional Implementation Details

D. Experiment Details

D.1. Theoretical Background of Benchmark Problems

MIS Problems There are some theoretical results for MIS problems on RRGs with the node degree set to d , where each node is connected to exactly d other nodes. First, for every d , a specific value ρ_d^* , which is dependent on only the degree d , exists such that the independent set density $|\mathcal{I}^*|/|V|$ converges to ρ_d^* with a high probability as N approaches infinity (Bayati et al., 2010). Second, a statistical mechanical analysis provides the typical MIS density ρ_d^{Theory} , as shown in Figure 2, and we clarify that for $d > 16$, the solution space of \mathcal{I} undergoes a clustering transition, which is associated with hardness in sampling (Barbier et al., 2013) because the clustering is likely to create relevant barriers that affect any algorithm searching for the MIS \mathcal{I}^* . Finally, the hardness is supported by analytical results in a large d limit, which indicates that, while the maximum independent set density is known to have density $\rho_{d \rightarrow \infty}^* = 2 \log(d)/d$, to the best of our knowledge, there is no known algorithm that can find an independent set density exceeding $\rho_{d \rightarrow \infty}^{\text{alg}} = \log(d)/d$ (Coja-Oghlan & Efthymiou, 2015).

MaxCut Problems This study has also focused on the MaxCut problems on d -RRGs, for which several theoretical results have been established. Specifically, for each d , the maximum cut ratio is given by $\nu_d^* \approx d/4 + P_* \sqrt{d/4} + \mathcal{O}(\sqrt{d})$, where $P_* = 0.7632\dots$ with a high probability as N approaches infinity (Parisi, 1980; Dembo et al., 2017). Thus, we take $\nu_d^{\text{UB}} = d/4 + P_* \sqrt{d/4}$ as an upper bound for the maximum cut ratio in the large n limit.

D.2. GNNs

A GNN (Gilmer et al., 2017; Scarselli et al., 2008) is a specialized neural network for representation learning of graph-structured data. GNNs learn a vectorial representation of each node in two steps, i.e., the aggregate and combine steps. The aggregate step employs a permutation-invariant function to generate an aggregated node feature, and in the combine step, the aggregated node feature is passed through a trainable layer to generate a node embedding, known as "message passing" or the "readout phase." Formally, for a given graph $G = (V, E)$, where each node feature $\mathbf{h}_v^{(0)} \in \mathbb{R}^{H^{(0)}}$ is attached to each node $v \in V$, the GNN updates the following two steps iteratively. First, the aggregate step at each l -th layer is defined as follows:

$$\mathbf{a}_v^{(l)} = \text{Aggregate}_{\theta}^{(l)} \left(\{ \mathbf{h}_u^{(l-1)}, \forall u \in \mathcal{N}_v \} \right), \quad (9)$$

where the neighborhood of $v \in V$ is denoted $\mathcal{N}_v = \{u \in V \mid (v, u) \in E\}$, $\mathbf{h}_u^{(l-1)}$ is the node feature of the neighborhood, and $\mathbf{a}_v^{(l)}$ is the aggregated node feature of the neighborhood. Then, the combined step at each l -th layer is defined as follows:

$$\mathbf{h}_v^{(l)} = \text{Combine}_{\theta}^{(l)} (\mathbf{h}_v^{(l-1)}, \mathbf{a}_v^{(l)}), \quad (10)$$

where $\mathbf{h}_v^{(l)} \in \mathbb{R}^{H^{(l)}}$ denotes the node representation at the l -th layer. Here, the hyperparameters for the total number of layers L and the intermediate vector dimension $N^{(l)}$ are determined empirically. Although numerous implementations of GNN architectures have been proposed to date, the most basic and widely used architecture is the GCN (Scarselli et al., 2008), which is given as follows:

$$\mathbf{h}_v^{(l)} = \sigma \left(W^{(l)} \sum_{u \in \mathcal{N}(v)} \frac{\mathbf{h}_u^{(l-1)}}{|\mathcal{N}(v)|} + B^{(l)} \mathbf{h}_v^{(l-1)} \right), \quad (11)$$

where $W^{(l)}$ and $B^{(l)}$ are trainable parameters, $|\mathcal{N}(v)|$ serves as a normalization factor, and $\sigma : \mathbb{R}^{H^{(l)}} \rightarrow \mathbb{R}^{H^{(l)}}$ is some component-wise nonlinear activation function, e.g., the sigmoid or ReLU function.

E. Additional Experiments

E.1. Ablation over Initial Scheduling Value and Scheduling Rate

We conducted an ablation study focusing on the initial scheduling value $\gamma(0)$ and scheduling rate ε . This numerical experiment was conducted under the configuration described in Section 3.1. Figure 7 shows the IS density of $N = 10000$

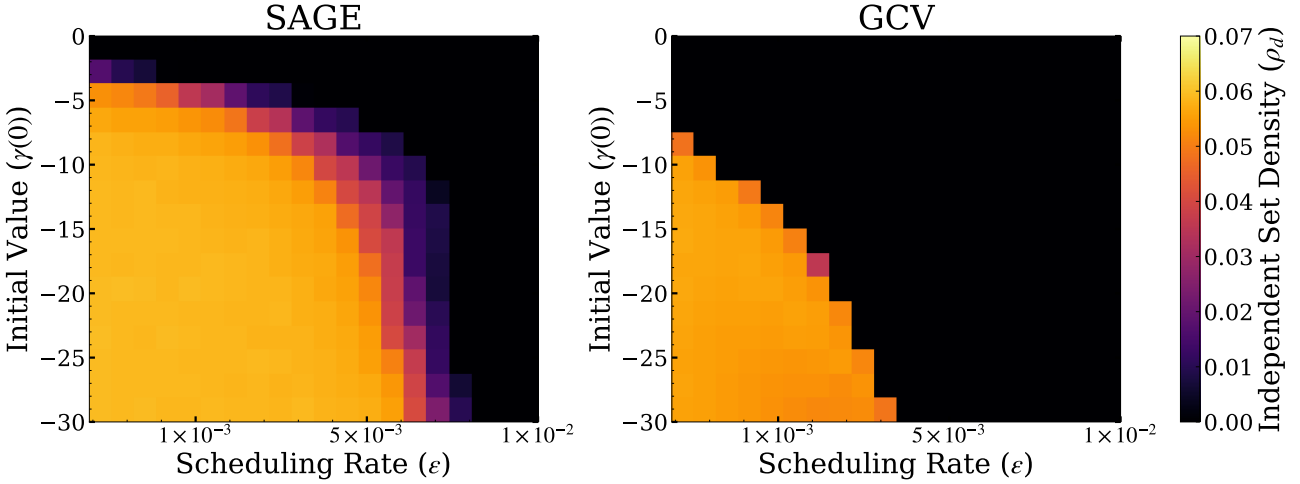


Figure 7. (Top) IS density of $N = 10,000$ MIS problems on 100-RRG as a function of initial scheduling $\gamma(0)$ and scheduling rate ε values obtained by the CRA-PI-GNN solver using GraphSage (Left) and GCV (Right). The color of the heat map represents the average IS over five different instances.

MIS problems on a 100-RRG as a function of the initial scheduling value $\gamma(0)$ and the scheduling rate ε using the CRA-PI-GNN with both GraphSage and GCV. As can be seen, smaller initial scheduling $\gamma(0)$ and scheduling rate ε values typically yield better solutions. However, the convergence time increases progressively as the initial scheduling $\gamma(0)$ and scheduling rate ε values become smaller. In addition, GraphSage consistently produces better solutions even with relatively larger initial scheduling $\gamma(0)$ and scheduling rate ε values, which implies that the GNN architecture influences both the solution quality and the effective regions of the initial scheduling $\gamma(0)$ and scheduling rate ε values for the annealing process.

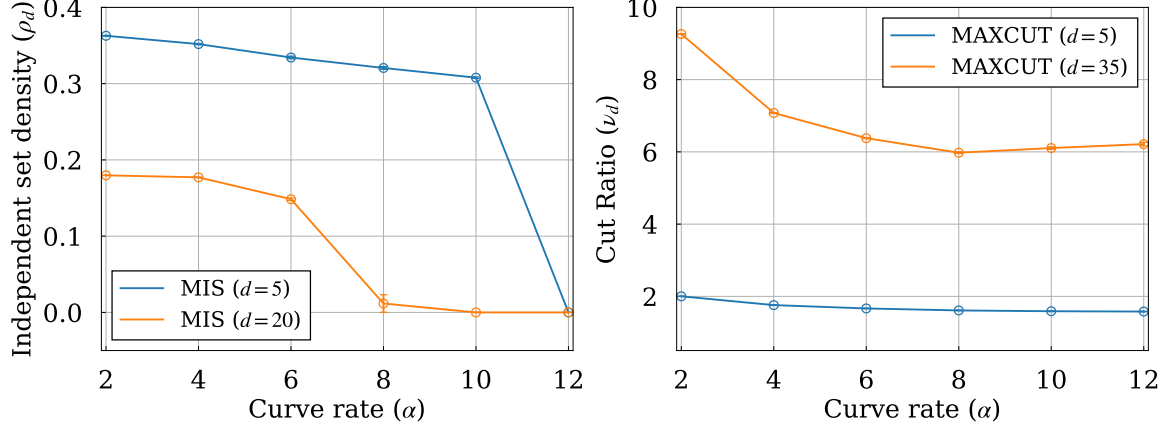


Figure 8. (Left) Independent set density as a function of curvature rate α in Eq. (6). (Right) Cut ratio as a function of curvature rate α in Eq. (6). Error bars represent the standard deviations of the results

E.2. Ablation over curve rate

Next, we investigated the effect of varying the curvature α in Eq. 6. Numerical experiments were performed on MIS problems with 10,000 nodes and the degrees of 5 and 20, as well as MaxCut problems with 10,000 nodes and the degrees of 5 and 35. The GraphSAGE architecture was employed, with other parameters set as Section 3.1. As shown in Figure 8, we observed that $\alpha = 2$ consistently yielded the best scores across these problems.